Materials Science and Engineering C 31 (2011) 1791–1799

Facile route to obtain a highly bioactive SiO_2–CaO–Na_2O–P_2O_5 crystalline powder

Renato Luiz Siqueira *, Edgar Dutra Zanotto

Laboratório de Materiais Vítreos, Departamento de Engenharia de Materiais Universidade Federal de São Carlos, Rod. Washington Luís km 235, CP 676, 13565-905 São Carlos, SP, Brazil

ARTICLE INFO

Article history:
Received 16 February 2011
Received in revised form 1 August 2011
Accepted 29 August 2011
Available online 2 September 2011

Keywords:
Bioactive ceramic
Solid-state reaction
Powder
SiO_2–CaO–Na_2O–P_2O_5
$Na_2Ca_2Si_3O_9$ crystal

ABSTRACT

This work describes a facile method to obtain highly bioactive crystalline powders of the SiO_2–CaO–Na_2O–P_2O_5 system using a simple route: solid state reaction. Success in obtaining the highly bioactive crystal phase of interest (sodium calcium silicate $Na_2Ca_2Si_3O_9$ containing phosphorus) involves heating the starting reactant powder mixture under an oxidizing atmosphere for 480 min in the temperature range 950–1000 °C. Despite a significant loss of phosphorus at heat treatment temperatures above 950 °C, the resulting $Na_2Ca_2Si_3O_9$ crystal phase is thermally stable up to 1100 °C. Longer treatment times favor the formation of a secondary phase (sodium calcium phosphate $NaCaPO_4$), which, according to recent studies, further increases the bioactivity of a similar material. Finally, in vitro bioactivity tests in acellular simulated body fluid (SBF) of a powder containing only the $Na_2Ca_2Si_3O_9$ phase has shown behavior similar to that of Biosilicate® — an ~99.5% crystalline glass–ceramic whose outstanding characteristics of interaction with living tissue have already been reported in the literature.

1. Introduction

The last few decades have been marked by intense research into the development of synthetic materials for tissue repair [1–3]. For instance, bioceramics have been widely tested for the repair or replacement of bones or parts due to their chemical similarity to bone and excellent biocompatibility [4,5]. Among these promising biomaterials, several bioactive glasses exhibit remarkable interaction with living tissues [6]. In addition to their bioactivity, i.e., their ability to form in situ a hydroxyapatite (HA) layer on their surfaces, which promotes a strong interface and bonds to cartilage and bones, it has been demonstrated that some bioactive glasses affect osteoblast activity and upregulate at least seven families of genes when primary human osteoblasts are exposed to their ionic dissolution products, including genes that encode proteins associated with osteoblast proliferation and differentiation [6–10].

However, despite the excellent potential of bioactive glasses to promote bone repair, their poor mechanical strength and toughness, their conchoidal (cutting) fracture and very limited machinability have restricted their use in several clinical applications. A strategy to substantially improve the mechanical performance of bioactive glasses for load-bearing implant devices has been their transformation into glass–ceramics by means of controlled internal crystallization. However, at the same time, the crystallization of some glassy systems significantly decreases their bioactivity. Hence, bioactive glasses generally present high bioactivity and low mechanical properties, whereas bioactive glass–ceramics have good mechanical properties but low bioactivity, such as those shown in Table 1 for some commercial materials [5,11,12].

Various types of glass–ceramics containing different crystalline phases have been developed to improve the mechanical strength and toughness of bioactive glasses. As demonstrated in Table 1, Cerabone® A/W, which contains apatite and wollastonite crystals in a MgO–CaO–SiO_2–P_2O_5 glass [5]; Ceravital®, which contains apatite in a Na_2O–K_2O–MgO–CaO–SiO_2–P_2O_5 glass [5,13]; and Bioverit®, which contains apatite and phlogopite in a Na_2O–MgO–CaO–Al_2O_3–SiO_2–P_2O_5–F glass [5,14,15] are some examples of commercial materials. These glass–ceramics have good mechanical properties but relatively low bioactivity indexes. The first bioactive glass–ceramic showing both good mechanical properties and high bioactivity index was developed in the mid-90s by Peitl et al. [16,17]. This monolithic bioactive glass–ceramic of the SiO_2–CaO–Na_2O–P_2O_5 system is about 30 to 65% crystalline, and its main phase is $Na_2Ca_2Si_3O_9$ with some phosphorus in solid solution and/or in the residual glassy phase.

The newest highly bioactive glass–ceramic based of the same SiO_2–CaO–Na_2O–P_2O_5 system, albeit with some compositional modifications and about 99.5% crystalline, was developed by Ravagnani and colleagues at the Vitreous Materials Laboratory of the Federal University of São Carlos, Brazil [18]. This almost fully crystalline glass–ceramic was patented and registered as Biosilicate® in 2003 [19]. Unlike all the other commercial bioactive glass–ceramics currently available (such as those shown in Table 1), the bioactivity of Biosilicate® is similar to that of the "gold standard" Bioglass® 45S5 developed by Hench in the early seventies [6]. Moreover, its mechanical properties are better than those of all existing highly bioactive glasses [20]. Due to its special characteristics, Biosilicate® has been tested successfully in several medical and dental applications [18,20–28].

* Corresponding author. Tel.: +55 16 3351 8556; fax: +55 16 3361 5404.
E-mail address: rastosfix@gmail.com (R.L. Siqueira).
URL: http://www.lamav.ufscar.br (R.L. Siqueira).

0928-4931/$ – see front matter © 2011 Elsevier B.V. All rights reserved.
doi:10.1016/j.msec.2011.08.013

Table 1
Bioactivity index and some of the mechanical properties of bioceramics used in clinical applications [5,11,12].

Bioceramics	Bioglass® 45S5	Bioglass® 52S4.6	Cerabone® A/W	Ceravital®	Bioverit® I
Bioactivity index (I_B)	12.5	10.5	6	5.6	$I_B<8$
Flexural strength (MPa)	40	40	215	100–150	140–180
Compressive strength (MPa)	?	?	1080	500	500
Young's modulus (GPa)	60	60	120	100–160	70–90
Structure	Glassy	Glassy	Apatite[a] Wollastonite Glassy phase	Apatite[a] Glassy phase	Phlogopite[a] Apatite[a] Glassy phase
Machinability	Low	Low	Fair	Fair	Good

?: data not found in the literature.
[a] composition not well defined.

After Peitl et al. [16,17] demonstrated the formation of the highly bioactive crystal phase $Na_2Ca_2Si_3O_9$ in some bioactive glass–ceramic compositions, several studies have reported the sintering and crystallization behaviors of Bioglass® 45S5 to obtain bioactive glass–ceramics in different forms (powders, monoliths and scaffolds for bone tissue engineering) [29–37]. It is interesting to note that in almost all these works the crystalline phase formation of greatest interest was $Na_2Ca_2Si_3O_9$, which significantly enhances the mechanical properties of the starting glass and maintains the high bioactivity of particular compositions of the SiO_2–CaO–Na_2O–P_2O_5 system. For instance, monolithic glass–ceramics showing bioactivity class A – biomaterial class A bonds to both hard (bone) and soft (cartilage) tissues –, fair machinability, low density (about 3 g cm^{-3}), good flexural strength (120–210 MPa), relatively low Young's modulus (70–80 GPa) and higher toughness than glass (1 MPa $m^{1/2}$) have been developed [16,20,27].

In the case of porous materials containing the same bioactive $Na_2Ca_2Si_3O_9$ crystal phase, Chen et al. [29] successfully synthesized highly porous (porosity: ~90%, cell diameter: 510–720 μm), mechanically competent (compressive strength: ~0.3–0.4 MPa), bioactive and biodegradable glass–ceramic scaffolds by the replication technique using Bioglass® 45S5 powder. According to these authors, the strength of 0.3–0.4 MPa is sufficient for the scaffold to be handled with, such as manipulating during in vitro bioactivity tests and cutting of the samples for mechanical tests. Bioglass® 45S5-derived glass–ceramic scaffolds with better compressive strengths (about 5.4–7.2 MPa) were prepared by Shih-Ching et al. [36] using the porogen burnout technique (with rice husks as an additive).

Another relevant issue to the present article is the fact that, starting with the works of Peitl et al. [16,17], the only route employed to obtain this highly bioactive crystal phase ($Na_2Ca_2Si_3O_9$) has been a traditional method that involves melting chemicals to obtain bioactive glasses, followed by controlled heat treatments that lead to their controlled crystallization [18,19,29,30,35–37]. Recently, Zhang et al. [38] published an interesting work, which experimentally investigates the equilibrium phase relations in the Na_2O–CaO–SiO_2 system at <50 wt.% SiO_2 concentrations at temperatures between 1200 and 1400 °C. Although the experimental results of their work may contribute for the complete understanding and thermodynamic modeling of the ternary Na_2O–CaO–SiO_2 phase diagram, the syntheses of the highly bioactive $Na_2Ca_2Si_3O_9$ crystal was not the authors' objective. Consequently, to the best of our knowledge, the preparation of this desirable crystal phase by facile route has not been proposed nor implemented up to this moment.

In 2007 we began a systematic study focusing on the synthesis of glassy and crystalline bioactive materials with compositions similar to those of Bioglass® 45S5 and Biosilicate® (materials of the same quaternary SiO_2–CaO–Na_2O–P_2O_5 system that show very high bioactivity indexes) using different chemical methods. In preliminary studies using the sol–gel method to prepare these materials [39,40] we were unable to obtain fully glassy materials, but the precipitation of the bioactive $Na_2Ca_2Si_3O_9$ crystal phase (albeit not in isolated form) was a significant result. With the sol–gel method established in that research we demonstrated the formation of this desirable phase in much milder laboratory conditions than the conventional glass–ceramic route, which involves melting, cooling and subsequent controlled crystallization. In the literature, we found only the work of Chen et al. [41] (published recently, after our work was concluded), which reports on the development of a sol–gel route for producing Na_2O-containing bioactive glass–ceramics with a composition similar to that of Bioglass® 45S5. These authors were more successful than we were in our initial studies and practically isolated the bioactive $Na_2Ca_2Si_3O_9$ crystal phase.

Considering this promising area of study and the importance of developing and producing bioceramics to reduce costs and create new (more effective, more durable and of wider social reach) alternatives for medical and dental treatments, our aim was to synthesize the highly bioactive $Na_2Ca_2Si_3O_9$ crystal phase using a simple and economically viable route: *solid state reaction*. This route was chosen because it is one of the most widely studied techniques employed industrially to obtain ceramic powders. It is a low cost technique and, in several cases, allows for the production of high-performance materials without requiring special apparatuses.

2. Experimental procedures

2.1. Preparation of the powders

The preparation of the highly bioactive $Na_2Ca_2Si_3O_9$ crystal phase containing phosphorus (possibly in solid solution) involved the decomposition and chemical reaction of silicon oxide (SiO_2; Vitrovita — PA), calcium carbonate ($CaCO_3$; J. T. Baker — PA), sodium carbonate (Na_2CO_3; J. T. Baker — PA) and sodium hydrogen phosphate (Na_2HPO_4; J. T. Baker — PA), according to pre-established compositions within the range 48–52 wt.% SiO_2: 22–25 wt.% CaO: 22–25 wt.% Na_2O: 2–6 wt.% P_2O_5 [16,17]. The reactant powders were weighed, mixed and homogenized for 12 h in a polyethylene terephthalate bottle (PET) using a planetary WAB Turbula T2C mixer. Individual portions containing approximately 20 g of uniformly mixed powder were heat-treated in ZAS crucibles (a zirconia, alumina, silica-based material).

The starting powder was heat-treated in an electric furnace at high temperatures under an oxidizing atmosphere (air). The heating program was determined based on the analytical results of previous differential thermal (DTA) and thermogravimetric (TG) analyses. The heat treatment consisted of heating at 10 K min^{-1}, followed by an isothermal hold at a temperature selected according to the data shown in Table 2. The samples were allowed to cool naturally in the electric furnace.

Upon completion of the heat treatments, the resulting poorly sintered agglomerates were crushed manually in an agate mortar and powders with particle sizes of 25 to 75 μm were selected and characterized. The flowchart in Fig. 1 outlines the procedure employed to prepare the powder and compares it with the two other procedures reported to obtain the highly bioactive $Na_2Ca_2Si_3O_9$ crystal phase.

2.2. In vitro bioactivity tests

To evaluate the bioactivity of the synthesized powders, we performed in vitro tests according to the method described by Kokubo et al. [5,42]. The solution employed in these tests, known as SBF (simulated body fluid), is acellular, protein-free and has a pH of 7.40. This solution is often used for the in vitro evaluation of the formation of a HA layer on the surface of materials designed for implants, according to ISO 23317: 2007 [43].

Table 2
Heat treatment program to convert the starting powder mixture into the highly bioactive $Na_2Ca_2Si_3O_9$ crystal phase.

Sample	Final treatment temperature (°C)	Duration (min)
Bio_1.1	800	30
Bio_1.2	800	60
Bio_1.3	800	120
Bio_1.4	800	240
Bio_1.5	800	480
Bio_2.5	850	480
Bio_3.5	900	480
Bio_4.5	950	480
Bio_5.5	1000	480
Bio_6.5	1050	480
Bio_7.5	1100	480
Bio_8.5	1000	960

2.2.1. Sample preparation

To test the in vitro bioactivity, the previously characterized powder (sample Bio_5.5), with particle sizes of 25 to 75 μm, was reformed into pellets with a 10 mm diameter and 2.3 mm in height. The reforming process consisted of two steps. First, the powders were pressed uniaxially at 65 MPa for 6 min with no agglutinant. The second step was performed in an isostatic press at 170 MPa for 3 min. Each pellet was suspended in SBF by a nylon string tied around its circumference. The pellets were cleaned ultrasonically for 15 s in acetone, dried, and then soaked in PET bottles containing SBF.

The volume of SBF used in the bioactivity tests is determined as a function of the sample's surface area. According to the procedures described by Kokubo et al. [5,42] for a dense material, the appropriate volume of solution should obey the following relationship:

$$V_s = S_a/_{10} \quad (1)$$

where V_s represents the volume of SBF (mL) and S_a represents the total geometric area of the sample (mm^2). For porous materials, such as the pressed pellets of this study, the aforementioned authors suggest the use of a volume higher than that calculated by Eq. (1). Therefore, in this work we used the following procedure: sample mass (m) divided by the volume of SBF (V_s) equal to 0.01 g mL^{-1}, since all the pellets had the same m. During the tests, the pellets were in contact with SBF for periods of 1, 2, 3, 6, 12, 24, 48, 72, 96, 120 and 144 h, and the system's temperature was kept at 37 °C, using the heating device illustrated in Fig. 2. After the predetermined test time, the pellets were taken out of their bottles and immersed in acetone for 10 s to remove the solution and stop surface reactions. Soon after drying, both pellet surfaces were analyzed to check for the formation of a HA surface layer.

2.2.2. Evaluation of sample solubility in SBF

To evaluate the solubility of the samples in SBF during the bioactivity tests, the ionic concentrations of H^+, Ca^{2+} and $P–PO_4^{3-}$ were analyzed an average of three times for each testing time. This enabled the identification of the dissolution behavior of the samples during the in vitro bioactivity tests. H^+ and Ca^{2+} were measured by the ion-selective electrode technique using a Roche cobas b121 electrolyte analyzer system. Ultraviolet and visible spectrophotometry (UV–Vis) were used for $P–PO_4^{3-}$ measurements, since inorganic phosphate ions in solution react with certain compounds, forming a blue chromophore whose color intensity is proportional to their concentration in the medium [44,45]. These measurements were taken with a Siemens ADVIA® 1800 clinical analyzer.

Samples of the highly bioactive glass–ceramic Biosilicate® (Vitrovita, São Carlos, SP, Brazil) in particulate form (showing the same particle size distribution as the Bio_5.5 sample) were also subjected to in vitro bioactivity tests under the same conditions described in Section 2.2 for a comparison with our material.

2.3. Instrumental analysis

2.3.1. Differential thermal analysis and thermogravimetry (DTA / TG)

DTA and TG analyses were performed in a Netzsch STA 409T instrument under an oxidizing atmosphere (synthetic air with a gas flow of 50 mL min^{-1}). Typical analyses involved samples of ~30 mg of the starting mixing powder and a heating program of 10 K min^{-1} from room temperature to 1000 °C to determine the initial heat treatment temperature to be applied in the powder preparations.

2.3.2. X-ray diffraction (XRD)

The crystalline phases resulting from the heat treatments of the powder mixtures were characterized by XRD. We used a Siemens D5000 diffractometer operating with CuKα radiation (λ = 0.15418 nm) and a filter system with a curved graphite secondary monochromator. The diffraction patterns were obtained in the 2θ range from 10° to 70° in continuous mode at 2° min^{-1}.

2.3.3. X-ray fluorescence spectrometry (XRF)

The composition of the synthesized powders was analyzed by XRF to evaluate possible compositional changes occurring in the samples during heat treatments. Samples with a particle size of <20 μm were selected and converted into glassy disks by melting in Pt–Au 5% crucibles (with the addition of a flux mixture containing 80 wt.% lithium metaborate and 20 wt.% lithium tetraborate). Composition measurements were performed in a Philips PW2404 sequential X-ray fluorescence spectrometer equipped with a rhodium X-ray tube.

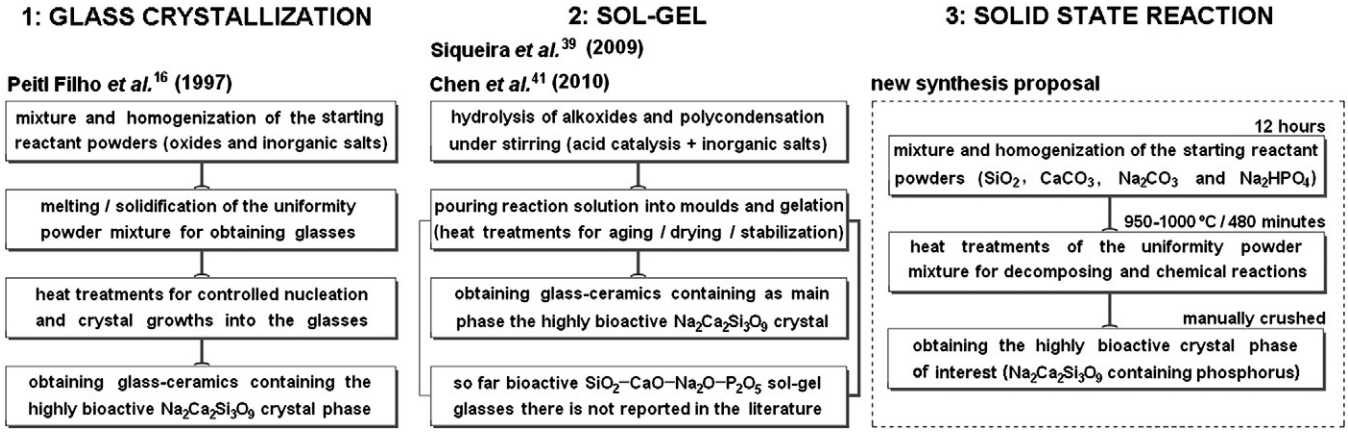

Fig. 1. Flowchart of the steps involved in preparing the highly bioactive $Na_2Ca_2Si_3O_9$ crystalline powders in comparison with the two other current routes (glass crystallization and sol–gel).

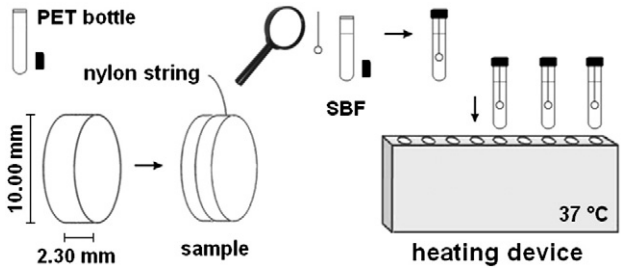

Fig. 2. Schematic representation of the procedures adopted for the in vitro bioactivity tests.

2.3.4. Fourier transform infrared spectroscopy (FTIR)

Pellet surface modifications after in vitro bioactivity tests were checked by FTIR, using a Perkin Elmer Spectrum GX spectrometer operating in reflectance mode with a 4 cm^{-1} resolution in the 4000–400 cm^{-1} region. FTIR spectra were also obtained from the synthesized powders, which, together with the X-ray diffraction patterns, allow for a more detailed analysis of the heat-treated powders.

2.3.5. Scanning electron microscopy and microanalysis (SEM/EDS)

The pellets were characterized morphologically by SEM to determine the surface modifications that occurred during the in vitro bioactivity tests. A set of samples was selected and analyzed before and after soaking in SBF for different testing times. The samples were coated with an evaporated gold film to render the surface electroconductive, and then analyzed under a Phillips FEG X-L30 microscope coupled to an energy dispersive X-ray spectrometer (EDS), which also allowed a qualitative chemical analysis of the samples' surfaces.

3. Results and discussion

3.1. Synthesis and characterization of the highly bioactive crystalline powders

3.1.1. Determination of the heat treatment program

The heat treatment program was selected based on simultaneous DTA and TG analyses of a portion of the reactant mixture containing SiO_2, $CaCO_3$, Na_2CO_3 and Na_2HPO_4 (homogenized for 12 h). The results of these analyses are shown in Fig. 3.

The starting powder mixture showed a mass loss of approximately 28%, becoming virtually stable at 900 °C, and remained in this condition until the final temperature of the test. From the beginning of the process up to 190 °C, approximately 2.5% of mass loss was attributed to the desorption of physically adsorbed water molecules on the surface of the powder particles. This initial low mass loss was due to the low hygroscopicity of the reactants, which makes them suitable for the synthesis method employed here. The most significant region was located between 190 and 900 °C, where practically all the phenomena of the process occurred. Due to their endothermicity, these phenomena were attributed to allotropic transformations and mainly decomposition of the reactants.

The first endothermic process illustrated in Fig. 3 (between 190 and 900 °C) was attributed to the decomposition of Na_2HPO_4 into sodium pyrophosphate and water ($Na_4P_2O_7 + H_2O_{(g)}$), which occurred in the temperature range of 190–270 °C [46–48]. The main product of the decomposition reaction, $Na_4P_2O_7$, remained practically stable until its melting temperature (988 °C) [49]. $CaCO_3$ undergoes allotropic transformations between 340 and 460 °C [47–50], decomposing into calcium oxide and carbon dioxide ($CaO + CO_{2\ (g)}$) between 620 and 850 °C [46,47]. In this case, CaO remained practically stable because its melting temperature is above 2500 °C [49]. Representing a considerable mass fraction in the starting powder mixture, the behavior of $CaCO_3$ in response to increasing temperature contributed significantly to the endothermic processes depicted in the DTA curve, and hence to the highest mass loss observed in the TG curve, which occurred between 600 and 900 °C.

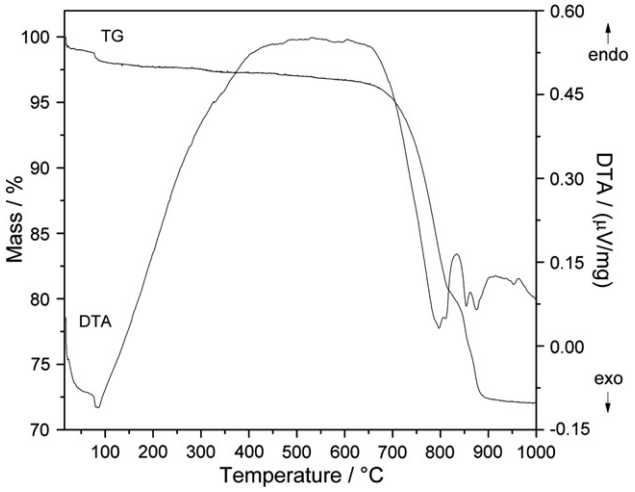

Fig. 3. DTA and TG curves of the starting reactant powder mixture.

On the other hand, Na_2CO_3 does not undergo a decomposition reaction such as that exhibited by $CaCO_3$ [51]. Na_2CO_3 undergoes allotropic transformations at 355, 485, 617 and 855 °C [50], the latter being the threshold of its melting temperature (856 °C) [49]. Thus, the endothermic processes observed near 850 °C in the graph of Fig. 3 may be related to its melting temperature, as well as to the decomposition of metastable phases formed in the system by the interaction between the reactant particles. SiO_2 has a melting temperature of 1722 °C [49] and contributes to the endothermic processes, exhibiting two allotropic transformations in the temperature range of the experiment; the first at approximately 570 °C and the other at 870 °C [49,52]. The much less pronounced endothermic processes detected above 900 °C were attributed to the decomposition of possible metastable phases formed in the system by chemical reactions, since the reactants do not undergo allotropic transformations above this temperature and there is no further evolution of volatiles, as can be verified in the TG curve.

Based on these observations, therefore, the initial heat treatment we chose consisted of heating the samples at 10 K min^{-1} up to 800 °C, followed by an isothermal heat treatment for 30 min, as described in Table 2. As the DTA and TG analyses in Fig. 3 show, the most intense processes in the system had already taken place below 800 °C, and there is evidence that chemical reactions between the particles of the starting powders begin near this temperature. The choice of the initial isothermal heat treatment of 30 min was arbitrary because our intention was to monitor the chemical reactions in the system from the very beginning.

3.1.2. The highly bioactive $Na_2Ca_2Si_3O_9$ crystal phase

To obtain the $Na_2Ca_2Si_3O_9$ crystal phase containing phosphorus (possibly in solid solution), every sample was heat-treated according to the program shown in Table 2. After any given heat treatment, the resulting powder was disaggregated and a portion containing particle sizes of 25 to 75 μm was analyzed by XRD before initiating a new treatment, obviously, with a new sample. Subsequently, the results of this analysis were checked and compared with the X-ray diffractogram of the mixed starting powder. Evidence of a reaction was only found from the heat treatment condition imposed on sample Bio_1.5 (800 °C/480 min). Based on this result, the time for the chemical reactions was kept constant at 480 min, while the temperature was increased progressively until a relatively stable phase (or phases) was obtained. Fig. 4 shows the X-ray diffractograms of the evolution of the phases formed as a function of the heat treatment temperature.

The X-ray diffractograms in Fig. 4 indicate that the heat treatment conditions established for the Bio_4.5 and Bio_5.5 samples sufficed to ensure no further changes occurred in the diffraction patterns. Thus, the powder resulting from the heat treatment of the Bio_4.5 sample (950 °C/480 min) remained virtually stable, as indicated by further heat treatment of a new Bio_5.5 sample at a higher temperature (1000 °C/480 min). In the diffractograms of samples Bio_1.1, Bio_1.2, Bio_1.3 and Bio_1.4 (diffractograms not shown), heat-treated at varying times and constant temperature, it should be noted that we were only able to identify some products of reactant decomposition, such as CaO and $Na_4P_2O_7$.

The X-ray diffractograms of Bio_4.5 and Bio_5.5 samples showed the exclusive formation of sodium calcium silicate ($Na_2Ca_2Si_3O_9$), with no other detectable phase. These diffractograms are shown comparatively in Fig. 5, indicating that they are in fairly good agreement along all the axes in the graph (only the peaks of highest intensity are highlighted). This successful result confirms the capability of the solid-state synthesis method to reproduce the highly bioactive $Na_2Ca_2Si_3O_9$ crystal phase containing phosphorus.

The intermediate phases formed in samples Bio_1.5, Bio_2.5 and Bio_3.5 were not characterized in detail. However, a preliminary analysis revealed the presence of calcium and sodium calcium silicates, although they could not be identified exactly.

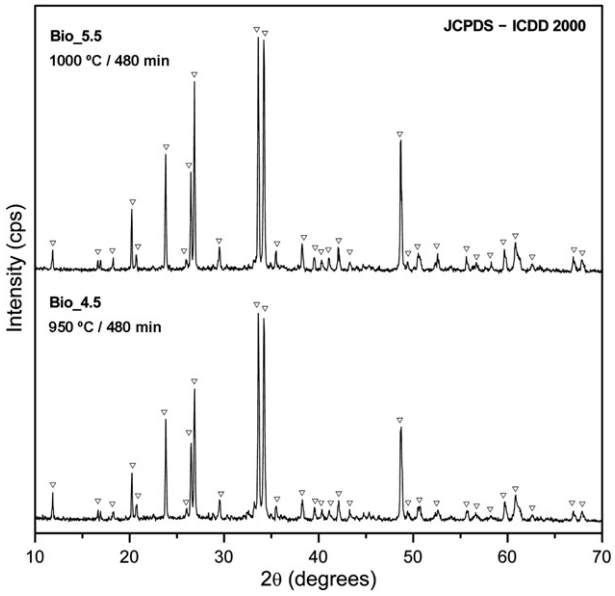

Fig. 5. XRD patterns of Bio_4.5 and Bio_5.5 samples. (▽ = $Na_2Ca_2Si_3O_9$).

3.1.3. Quantitative chemical analysis

Table 3 lists the results of the quantitative chemical analysis of the Bio_4.5 and Bio_5.5 samples performed by XRF.

In general, the nominal chemical composition established for the synthesis of the crystalline powders was in good agreement with the analyzed chemical compositions of the Bio_4.5 and Bio_5.5 samples. However, one aspect deserves further attention. As can be seen in Table 3, the conditions in which the Bio_5.5 sample was synthesized led to a significant loss of phosphorus (~60 wt.%). To confirm this result, a new *Bio_5.5 sample was prepared and synthesized under the same conditions (1000 °C/480 min) for a comparative XRF analysis. The results of this new *Bio_5.5 sample confirmed the higher loss of phosphorus at heat treatments above 950 °C. In addition, the Bio_4.5 sample showed the greatest loss on ignition, possibly attributable to the beginning of the evolution of phosphorus volatile species when the temperature increased from 950 °C to 1000 °C during the sample's preparation for the XRF analysis.

3.1.4. Thermal stability of the $Na_2Ca_2Si_3O_9$ crystal phase

To evaluate the thermal stability of the $Na_2Ca_2Si_3O_9$ crystal phase containing phosphorus, three new synthesis conditions were established, as shown in Table 2. Initially, the isothermal heat treatment time was kept constant at 480 min while the final temperature was increased to 1050 and 1100 °C. The X-ray diffractograms of the samples subjected to these new heat treatment conditions are shown in Fig. 6 and compared with the Bio_4.5 and Bio_5.5 samples.

According to the XRD patterns in Fig. 6, the $Na_2Ca_2Si_3O_9$ phase remained virtually stable after 480 min at 950, 1000, 1050 and 1100 °C. In the last treatment condition, the isothermal heat treatment temperature was set at 1000 °C, and the chemical reaction time increased from 480 to 960 min. The X-ray diffractogram of the

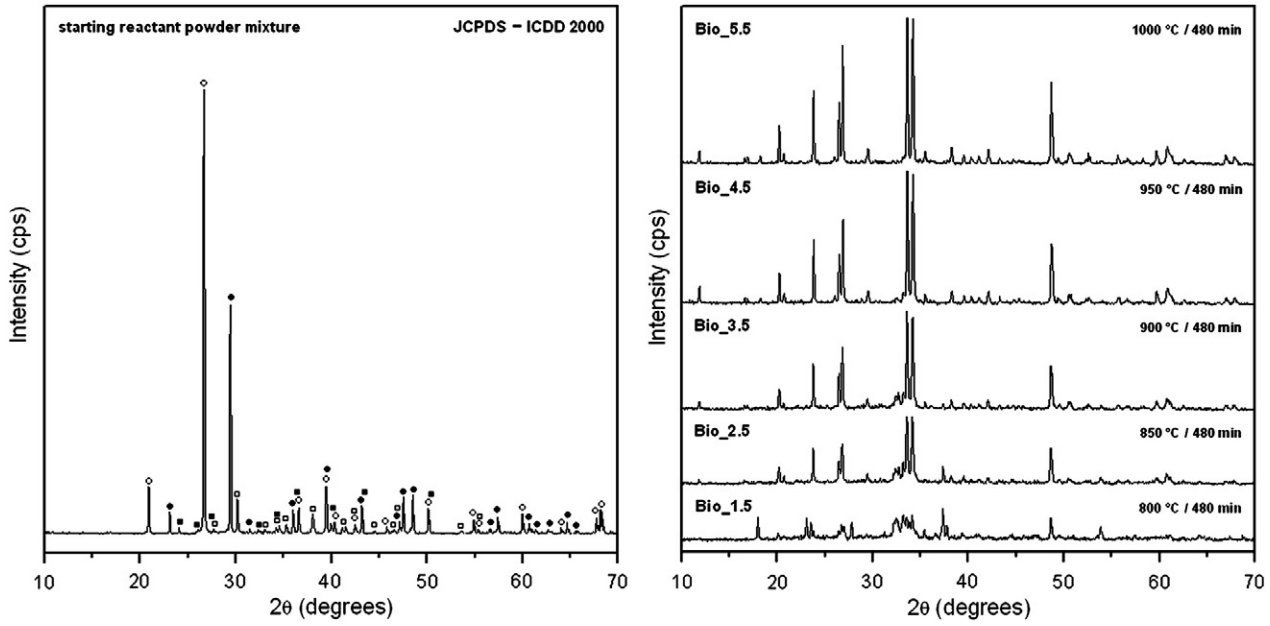

Fig. 4. XRD patterns of the starting reactant powder mixture and samples subjected to different heat treatment conditions to verify the formation of new phases. (○ = SiO_2; ● = $CaCO_3$; □ = Na_2CO_3; ■ = Na_2HPO_4).

Table 3
Quantitative XRF chemical analysis of Bio_4.5 and Bio_5.5 samples.

Composition	Nominal	Bio_4.5	Bio_5.5	*Bio_5.5
% SiO_2	48–52	46.7	50.3	49.9
% CaO	22–25	22.7	24.2	23.9
% Na_2O	22–25	25.4	23.5	24.1
% P_2O_5	2–6	4.2	1.6	1.4
% MnO	–	<0.003	<0.003	<0.003
% MgO	–	<0.01	<0.01	<0.01
% TiO_2	–	0.02	0.01	0.03
% Al_2O_3	–	<0.01	<0.01	<0.01
% K_2O	–	0.06	0.05	0.06
% Fe_2O_3	–	0.03	0.03	0.03
% Loss on ignition (1000 °C)	–	0.75	0.17	0.23

%: value expressed in weight.
*: new sample Bio_5.5.

sample subjected to this heat treatment is shown in Fig. 7 and compared with all the other samples.

The diffractogram of the Bio_8.5 sample showed no significant difference from the diffractograms of the other samples, as shown in Fig. 7. The increase in heat treatment temperature and time for chemical reactions did not affect the resulting powders, indicating good thermal stability of the $Na_2Ca_2Si_3O_9$ crystal phase. An important factor that should be considered is the loss of phosphorus in the samples subjected to these heat treatments. We previously demonstrated a significant loss of phosphorus in samples heat-treated at 1000 °C for 480 min. Therefore, it would be reasonable to expect higher losses in the Bio_6.5 (1050 °C/480 min), Bio_7.5 (1100 °C/480 min) and Bio_8.5 (1000 °C/960 min) samples subjected to these new heat treatment conditions. But the potential loss of phosphorus in these samples was not determined.

With regard to the heat treatment conditions established for the Bio_4.5, Bio_5.5, Bio_6.5, Bio_7.5 and Bio_8.5 samples, it is clear from the X-ray diffraction patterns that no significant changes in the resulting powders were detectable. However, the complementary FTIR results indicated small, albeit important, changes. Fig. 8 shows the FTIR spectra of these samples, revealing the effect of the increased heat treatment temperature and time.

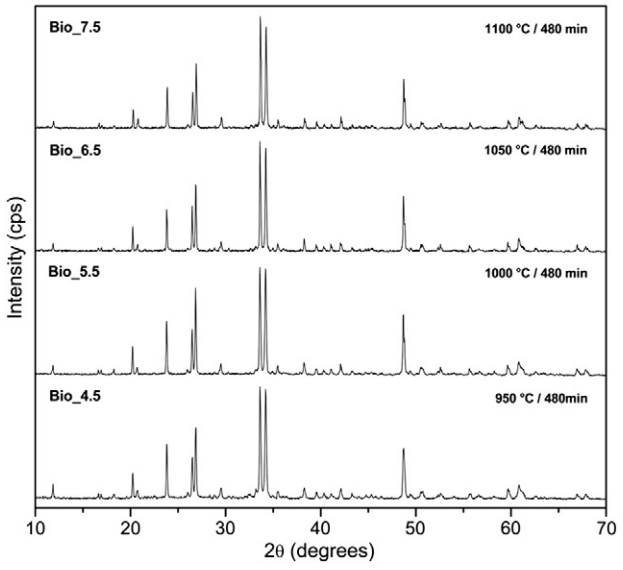

Fig. 6. XRD patterns of samples subjected to different heat treatment conditions to verify the thermal stability of the $Na_2Ca_2Si_3O_9$ crystal phase: influence of the heat treatment temperature.

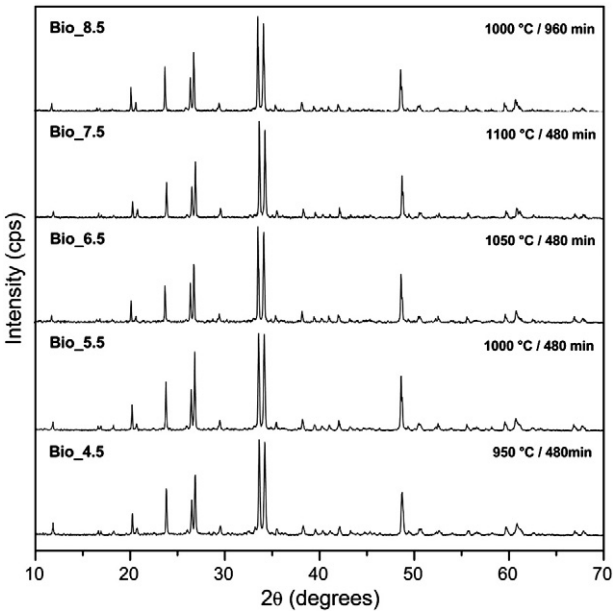

Fig. 7. XRD patterns of samples subjected to different heat treatment conditions to verify the thermal stability of the $Na_2Ca_2Si_3O_9$ crystal phase: influence of the heat treatment time.

The FTIR spectra of all the samples shown in Fig. 8 are characterized mainly by intense bands in the region between 400 and 550 cm^{-1}, associated with the vibrational mode of δSi – O – Si bonds [17,18,21,37,40]. Bands related to the vibrational mode of νSi – O bonds appear near 620 cm^{-1} [18,21] and in the region between 900 and 1200 cm^{-1} [17,18,21,37,40]. In response to increased heat treatment temperature, a minor new band located close to 575 cm^{-1} appeared in the spectra of the Bio_6.5 and Bio_7.5 samples (see Fig. 8 item a). Crovace et al. [53] demonstrated that this small change in the spectrum was associated to a secondary crystal phase ($NaCaPO_4$) precipitated in the material. According to these authors, the presence of this phase considerably enhances the in vitro bioactivity of Biosilicate®.

The effect of heat treatment time was more pronounced than that of temperature, as can be seen in Fig. 8 (item b). The spectrum of the sample heat-treated at 1000 °C for 960 min (Bio_8.5 sample) shows a much more intense band related to the secondary $NaCaPO_4$ crystal phase at ~575 cm^{-1}. In addition, another band related to this phase appeared at ~510 cm^{-1}, while the bands associated with the vibrational mode of δSi – O – Si and νSi – O bonds were less intense.

3.2. Preliminary in vitro bioactivity tests

3.2.1. Evaluation of the formation of a HA layer on the samples' surfaces

In these preliminary in vitro bioactivity tests, all the pressed powder pellets of Bio_5.5 and Biosilicate® samples exhibited a HA layer on their surfaces starting from a testing time of 24 h, as indicated in the FTIR spectra in Fig. 9.

As can be seen from the FTIR spectra of the samples exposed to SBF, a significant change occurred on the samples' surfaces (spectra not shown) starting from 3 h of testing. These spectral changes can be attributed to stages 1, 2, 3 and 4 of the proposed mechanism for bioactivity, which culminates in the formation of an amorphous calcium phosphate layer (amorphous CaP) on the samples' surfaces [4,5,11,12,17,21]. All the spectra obtained after more than 24 h of testing were analogous to the spectrum of synthetic HA, exhibiting, as a function of testing time, only changes relating to the intensity of the characteristic HA bands located in the vicinity of 570, 610, 1050 and 1130 cm^{-1} [5,17,18,21].

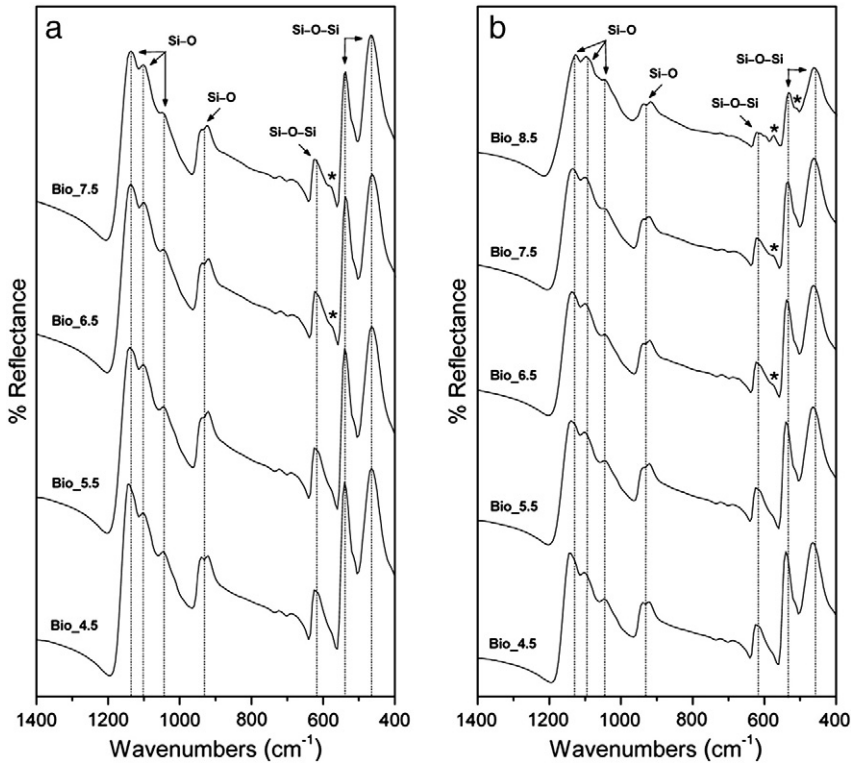

Fig. 8. FTIR spectra of samples subjected to different heat treatment conditions to verify the thermal stability of the $Na_2Ca_2Si_3O_9$ crystal phase: (a) influence of the heat treatment temperature; (b) influence of the heat treatment time. (∗ = $NaCaPO_4$) [53].

Fig. 10 shows the morphologies of some of the pellets and their respective qualitative chemical analysis before and after exposure to SBF for 96 h. All the samples tested for more than 24 h exhibited the typical morphology of HA [5,42]. The EDS spectra of these samples revealed a major compositional change on their surfaces after 96 h of testing (with the predominance of Ca and P). The EDS analysis, which indicated that this significant compositional change occurred on the surfaces of all the samples tested for more than

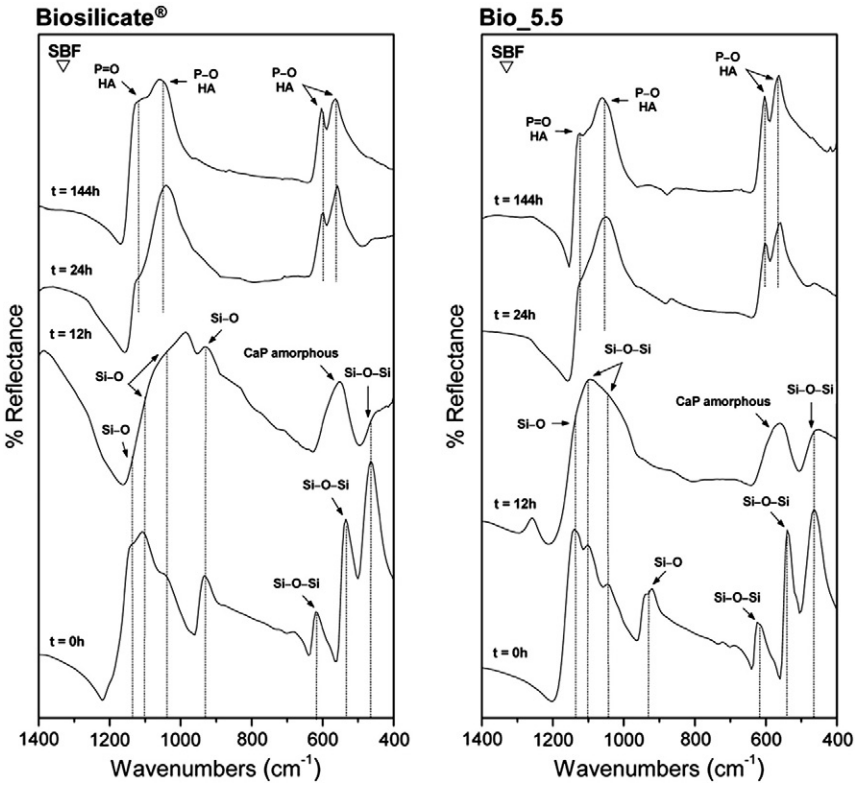

Fig. 9. FTIR spectra of several Biosilicate® and Bio_5.5 sample surfaces before and after soaking in SBF for different testing times.

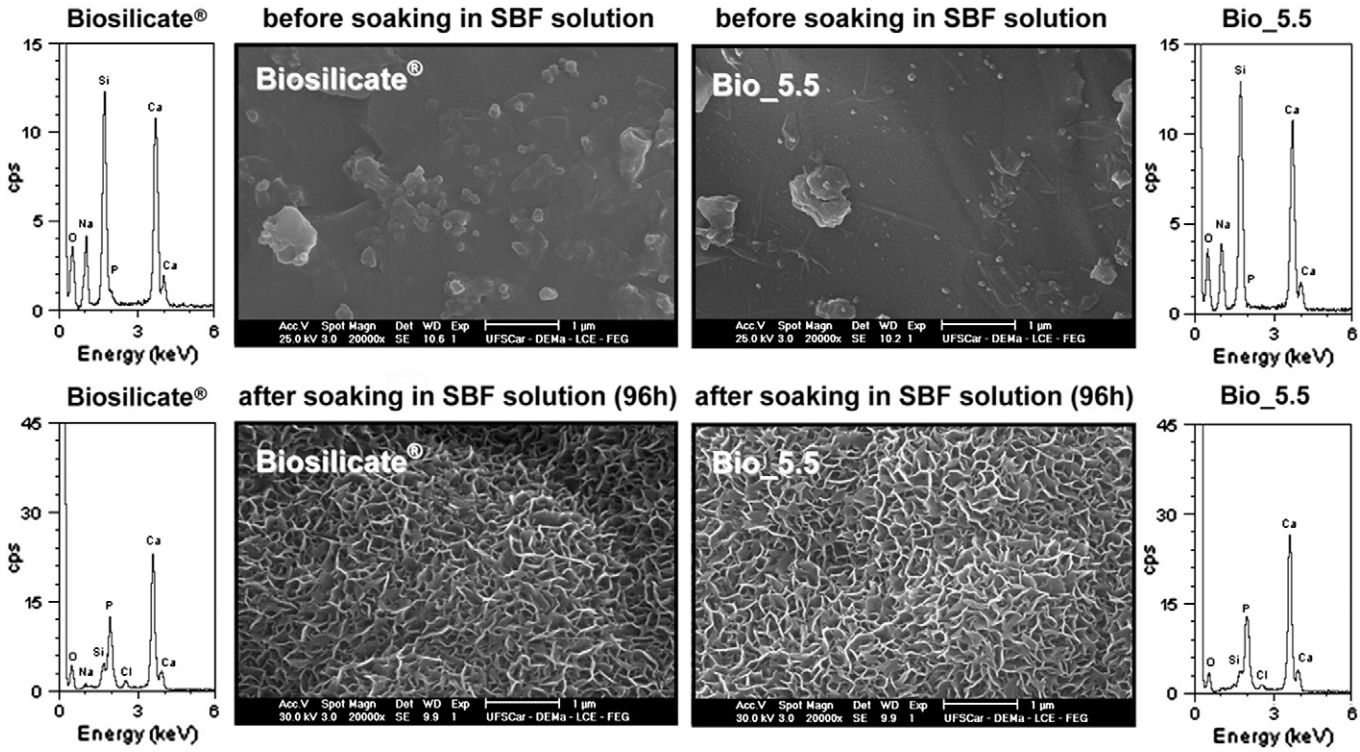

Fig. 10. SEM micrographs and EDS spectra of Biosilicate® and Bio_5.5 sample surfaces: before and after soaking in SBF for 96 h.

24 h, was consistent with the FTIR spectra, confirming the formation of a HA layer.

3.2.2. Evaluation of the sample's solubility in SBF

Fig. 11 shows the variation in pH and calcium and phosphorus concentrations as a function of the exposure time of pressed powder pellets of Bio_5.5 and Biosilicate® samples to SBF. As these results indicate, the two samples showed a very similar behavior in SBF. In the first 24 h of testing, the pH increased from 7.4 to approximately 7.8. The pH of the SBF increased due to the ionic exchange between H^+ and Ca^{2+} concentrations in response to the rapid dissolution of the material. In this same time period, the Ca^{2+} concentration presented a

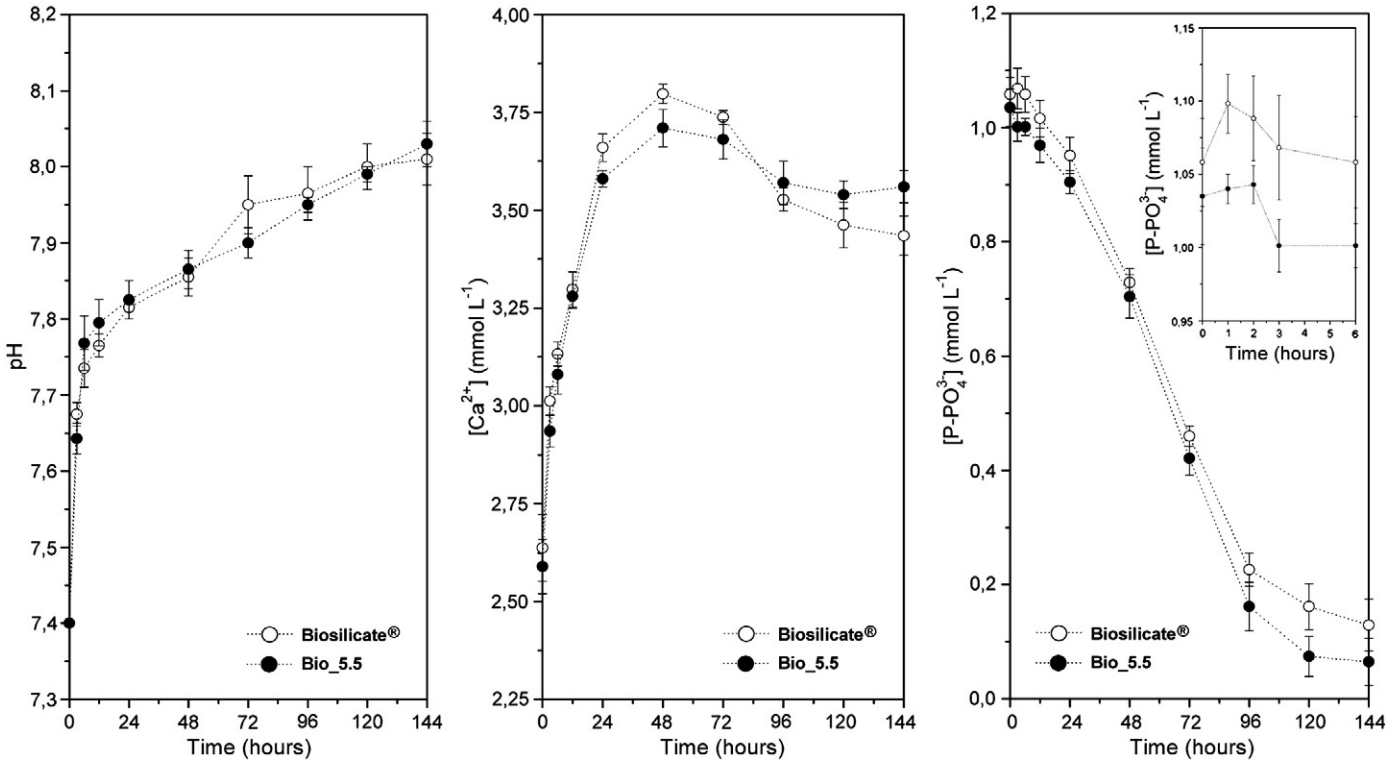

Fig. 11. Variation in pH and calcium and phosphorus concentrations as a function of exposure time of Biosilicate® and Bio_5.5 samples to SBF.

variation of approximately 1.2 mmol L^{-1}. After 24 h of testing, the Ca^{2+} concentration fluctuated, showing a declining trend. The total Ca^{2+} variation in SBF during the test was around 1.0 mmol L^{-1}, while the pH of both samples reached values of approximately 8.1. The concentration of P–PO_4^{3-} decreased considerably after 3 h of testing, and was almost depleted after testing times of over 96 h. This consumption was due to the early formation of amorphous CaP on the surface of the samples, and its subsequent evolution to HA (see Fig. 9). These steps depended almost exclusively on the phosphorus provided by SBF, since it was only possible to detect the increase in P–PO_4^{3-} from the mid-point to the end of 3 h of testing time, as shown in Fig. 11 (this trend was more evident with Biosilicate®, probably because of its higher phosphorus concentration than the Bio_5.5 sample).

The results obtained from these preliminary in vitro bioactivity tests of the Bio_5.5 sample are very significant because Biosilicate® has been widely recognized for its high bioactivity in both in vitro and in vivo conditions [18–28,53].

4. Conclusions

Highly bioactive crystalline powders of the SiO_2–CaO–Na_2O–P_2O_5 system were synthesized using a facile route: solid state reaction. This synthesis process requires moderate temperatures and only a few hours to obtain the bioactive crystal phase of interest (sodium calcium silicate $Na_2Ca_2Si_3O_9$ containing phosphorus).

The solid-state synthesis method developed here is quite feasible and much simpler than the two other current routes (glass crystallization and sol–gel) already established to obtain this particular bioactive crystal phase in particulate form. Due to the simple processing, low cost and potential advantages of this method for large-scale production, the results produced in this study may contribute to the industrial manufacture of this highly bioactive material.

Acknowledgments

The authors thank Dr. Helder Biz for his valuable input and discussions, and Vitrovita (Glass-Ceramic Innovation Institute, São Carlos, SP, Brazil) for providing samples of Biosilicate® and for the use of its equipment. We also gratefully acknowledge the Brazilian funding agency FAPESP — Fundação de Amparo à Pesquisa do Estado de São Paulo — (grant # 2007/08179-0) for the financial support of this research project.

References

[1] E.S. Place, N.D. Evans, M.M. Stevens, Nat. Mater. 8 (2009) 457–470.
[2] D.F. Williams, Biomaterials 30 (2009) 5897–5909.
[3] R.J. Narayan, Philos. Trans. R. Soc. Lond. A 368 (2010) 1831–1837.
[4] L.L. Hench, J. Am. Ceram. Soc. 81 (1998) 1705–1728.
[5] T. Kokubo, Bioceramics and Their Clinical Applications, CRC Press, Boca Raton, 2008.
[6] L.L. Hench, J. Mater. Sci. Mater. Med. 17 (2006) 967–978.
[7] P. Valério, M.M. Pereira, A.M. Goes, M.F. Leite, Biomaterials 25 (2004) 2941–2948.
[8] M. Bosetti, M. Cannas, Biomaterials 26 (2005) 3873–3879.
[9] L.L. Hench, J. Eur. Ceram. Soc. 29 (2009) 1257–1265.
[10] O. Tsigkou, J.R. Jones, J.M. Polak, M.M. Stevens, Biomaterials 30 (2009) 3542–3550.
[11] L.L. Hench, Biomaterials 19 (1998) 1419–1423.
[12] P.N. De Aza, A.H. De Aza, P. Pena, S. De Aza, Bol. Soc. Esp. Ceram. 46 (2007) 45–55.
[13] H. Brömer, K. Deutscher, B. Blenke, E. Pfeil, V. Strunz, Sci. Ceram. 9 (1977) 219–223.
[14] W. Höland, W. Vogel, K. Naumann, J. Gummel, J. Biomed. Mater. Res. 19 (1985) 303–312.
[15] W. Vogel, J. Non-Cryst. Solids 73 (1985) 593–597.
[16] O. Peitl, E.D. Zanotto, G.P. La Torre, L.L. Hench, Bioactive ceramics and method of preparing bioactive ceramics, Patent WO/1997/041079, November 06, 1997.
[17] O. Peitl, E.D. Zanotto, L.L. Hench, J. Non-Cryst. Solids 292 (2001) 115–126.
[18] C. Ravagnani, Biosilicate for oral health promotion, Master of Science Dissertation, Federal University of São Carlos, Brazil, 2003 (supervisors E.D. Zanotto and O. Peitl).
[19] E.D. Zanotto, C. Ravagnani, O. Peitl, H. Panzeri, E.H.G. Lara, Process and compositions for preparing particulate, bioactive or resorbable biosilicates for use in the treatment of oral ailments, Patent WO/2004/074199, September 02, 2004.
[20] R.L. Siqueira, E.D. Zanotto, Quím. Nova 34 (2011) 1231–1241.
[21] J. Moura, L.N. Teixeira, C. Ravagnani, O. Peitl, E.D. Zanotto, M.M. Beloti, H. Panzeri, A.L. Rosa, P.T. Oliveira, J. Biomed. Mater. Res. 82 (2007) 545–557.
[22] R.N. Granito, D.A. Ribeiro, A.C.M. Renno, C. Ravagnani, P.S. Bossini, O. Peitl, E.D. Zanotto, N.A. Parizotto, J. Oishi, J. Mater. Sci. Mater. Med. 20 (2009) 2521–2526.
[23] E.T. Massuda, L.L. Maldonado, J.T. Lima Júnior, O. Peitl, M.A. Hyppolito, J.A. Oliveira, Braz. J. Otorhinolaryngol. 75 (2009) 665–668.
[24] R.O. Jabur, A.E. Trivellato, O. Peitl, V.M.R. Barros, Oral Surg. 2 (2009) 161–166.
[25] V.M. Roriz, A.L. Rosa, O. Peitl, E.D. Zanotto, H. Panzeri, P.T. Oliveira, Clin. Oral Implants Res. 21 (2010) 148–155.
[26] A.C.M. Renno, P.A. McDonnell, M.C. Crovace, E.D. Zanotto, L. Laakso, Photomed. Laser Surg. 28 (2010) 131–133.
[27] E.D. Zanotto, Am. Ceram. Soc. Bull. 89 (2010) 19–27.
[28] C. Tirapelli, H. Panzeri, E.H.G. Lara, R.G. Soares, O. Peitl, E.D. Zanotto, J. Oral Rehabil. 38 (2011) 253–262.
[29] Q.Z. Chen, I.D. Thompson, A.R. Boccaccini, Biomaterials 27 (2006) 2414–2425.
[30] A.R. Boccaccini, Q. Chen, L. Lefebvre, L. Gremillard, J. Chevalier, Faraday Discuss. 136 (2007) 27–44.
[31] R. Huang, J. Pan, A.R. Boccaccini, Q.Z. Chen, Acta Biomater. 4 (2008) 1095–1103.
[32] O. Bretcanu, C. Samaille, A.R. Boccaccini, J. Mater. Sci. 43 (2008) 4127–4134.
[33] L. Lefebvre, L. Gremillard, J. Chevalier, R. Zenati, D. Bernache-Assolant, Acta Biomater. 4 (2008) 1894–1903.
[34] Q.Z. Chen, A. Efthymiou, V. Salih, A.R. Boccaccini, J. Biomed. Mater. Res. A 84 (2008) 1049–1060.
[35] H. Arstila, L. Hupa, K.H. Karlsson, M. Hupa, J. Non-Cryst. Solids 354 (2008) 722–728.
[36] W. Shih-Ching, H. Hsueh-Chuan, H. Sheng-Hung, H. Wen-Fu, J. Mater. Sci. Mater. Med. 20 (2009) 1229–1236.
[37] O. Bretcanu, X. Chatzistavrou, K. Paraskevopoulos, R. Conradt, I. Thompsond, A.R. Boccaccini, J. Eur. Ceram. Soc. 29 (2009) 3299–3306.
[38] Z. Zhang, Y. Xiao, J. Voncken, Y. Yang, R. Boom, N. Wang, Z. Zou, J. Am. Ceram. Soc. 94 (2011) 3088–3093.
[39] R.L. Siqueira, O. Peitl, E.D. Zanotto, 15th International Sol-Gel Conference, Abstracts Book, Porto de Galinhas, Brazil, 2009.
[40] R.L. Siqueira, O. Peitl, E.D. Zanotto, Mater. Sci. Eng. C 31 (2011) 983–991.
[41] Q.-Z. Chen, Y. Li, L.-Y. Jin, J.M.W. Quinn, P.A. Komesaroff, Acta Biomater. 6 (2010) 4143–4153.
[42] T. Kokubo, H. Takadama, Biomaterials 27 (2006) 2907–2915.
[43] ISO 23317, Implants for surgery: *in vitro* evaluation for apatite-forming ability of implant materials, June 2007.
[44] C.H. Fiske, Y. Subbarow, J. Biol. Chem. 66 (1925) 375–400.
[45] G. Gomori, J. Lab. Clin. Med. 21 (1942) 955–960.
[46] C.H. Bamford, C.F.H. Tipper, Reactions in the Solid State Vol. 22, Elsevier Science, Amsterdam, 1980.
[47] A.K. Galwey, M.E. Brown, Thermal Decomposition of Ionic Solids Vol. 86, Elsevier Science, Amsterdam, 1999.
[48] T. Iida, N. Takai, T. Yamabe, Bull. Chem. Soc. Jpn. 44 (1971) 686–688.
[49] D.R. Lide, Handbook of Chemistry and Physics, 87th ed. CRC Press, Boca Raton, 2007.
[50] K.H. Stern, High Temperature Properties and Thermal Decomposition of Inorganic Salts with Oxyanions, CRC Press, New York, 2001.
[51] A.S. Maia, V.K.L. Osorio, Quím. Nova 26 (2003) 595–601.
[52] J.F. Shackelford, R.H. Doremus, Ceramic and Glass Materials: Structure, Properties and Processing, Springer, New York, 2008.
[53] M.C. Crovace, Sintering of Biosilicate® for synthesis of highly bioactive porous structures, Master of Science Dissertation, Universidade Federal de São Carlos, Brazil, 2009 (supervisor A.C.M. Rodrigues).